

Short life fission products extracted from molten salt reactor fuel for radiopharmaceutical applications.

Claude Degueldre*, Joshua Findlay, David Cheneler, Suneela Sardar, Sarah Green.

School of Engineering, Lancaster University, Lancaster LA1 4YW, UK

*Corresponding author: c.degueldre@lancaster.ac.uk

Abstract

This work studies the potentialities of short life fission product (^{A}Fp) radioisotopes e.g. ^{82}Br , ^{86}Rb , (^{90}Sr) - $^{90\text{m}}\text{Y}$, (^{99}Mo) - $^{99\text{m}}\text{Tc}$, ^{103}Ru - $^{103\text{m}}\text{Rh}$, ^{111}Ag , ^{127}Sb - $^{127(\text{m})}\text{Te}$, ^{126}I , ^{131}I , ^{133}Xe , ^{136}Cs , ^{141}Ce , ^{143}Ce , ^{143}Pr , ^{147}Nd - ^{147}Pm , ^{149}Pm , ^{153}Sm , ^{156}Eu , ^{159}Gd and ^{161}Tb , extracted from a molten salt reactor and their separation using specific thermodynamic and radiochemical conditions. Their utilisation by coupling radio-diagnostics and radiotherapy is emphasised. A molten salt reactor produces fission products during operation. These radioisotopes can be separated at line from the liquid fuel applying careful separation by evaporation/distillation, chemical reduction (using H_2 doped gas), electro-deposition and/or chemical oxidation (using Cl_2 doped gas). They can be refined and chemically treated for radiopharmaceutical use for diagnostics utilising γ radioscopy or positron emission tomography and potentially in radiotherapy for specific tumorous affected organ or viral diseases using β^- emitters.

Among these ^{A}Fp isotopes currently used for diagnostics thanks to their emitted γ rays of energy 50-200 keV, some may also be used for radiotherapy of the diagnosed organ utilising their β^- ($E_{\text{Mean}} \approx 100$ keV) whose mean free pathway of 100 nm in biological tissue is much smaller than the penetration depth of these β^- . Emphasis is finally given for ^{86}Rb , ^{90}Y , $^{99\text{m}}\text{Tc}$, ^{131}I and ^{133}Xe as well as on the ^{A}Ln isotopes (^{141}Ce , ^{143}Ce - ^{143}Pr , ^{147}Nd - ^{147}Pm , ^{149}Pm and ^{153}Sm) because of their strong potential for complexation with bio-ligands (e.g. DOTA) or for their ability for micro- nano-sphere formation and because of their potential dual ability of imaging for diagnostic and as suggested radio-therapeutic vector for specific affections or of viral and bacterial diseases. These radio-lanthanides could also replace ^{177}Lu for the treatment of prostate cancer.

Keywords: Molten Salt Reactor; short life fission product radioisotopes; radio-diagnostics; radiotherapy.

1. Introduction

Since more than 50 years radio-pharmaceutical agents using radionuclides has been a growing field for medical research including passive imaging and radiotherapy as reported by Crestoni (2018) [1] in a last review. As reported by the author, this coupled approach exploits fast and non-invasive methodologies for:

- (i) 'Radio-diagnostic imaging of several diseases and real-time clinical monitoring via single-photon emission computed tomography and positron emission tomography e.g. Baarsgaard Hansen, & Bender, (2021) [2]' and
- (ii) 'Radiotherapy via emission of particulate, ionizing radiation, alpha (α) and beta (β^-) particles, and Auger electrons, depositing energy in tissues and causing cell death or virus resorption'.

Several nuclides for imaging (^{99m}Tc , ^{89}Zr , ^{111}In) and for radiotherapy (^{90}Y , ^{131}I , ^{153}Sm , ^{188}Re , ^{223}Ra , ^{225}Ac), are fission products, have been used to label pharmaceuticals molecules which are presently approved or are under radiopharmaceutical trials. General information on nuclear medicine technology can be found in the review authored by Bolus & Glasgow (2018) [3].

These radionuclides are usually made of activation products generated by irradiations using accelerators e.g. using (p,n) reactions producing light radioisotopes, or using nuclear reactors e.g. with (n, γ) reactions producing heavier radioisotopes than the reagent nuclide. Usually, research reactor e.g. Petten, are used for these productions which also requires separation by chemical approaches or by physical means as reported by Sun (2021) [4]. Since the cost of irradiation is of the order of £ 100 k per mole of neutron, it is suitable for economic reason to produce fission products in the frame of reactor operation without affecting the energy production as it would be the case in a light water reactor.

Fission product radioisotopes may consequently be extracted at line from the liquid fuel of molten salt reactor during treatment as precipitate or as quasi-volatile fission products. These fission product elements are in principle part of the radioactive waste materials. However, these isotopes should not be considered as nuclear waste materials since they are at least acknowledged for their medical applications as diagnostic based reagents in nuclear medicine. Among them, ^{82}Br , ^{86}Rb , (^{90}Sr) - ^{90m}Y , (^{99}Mo) - ^{99m}Tc , ^{103}Ru - ^{103m}Rh , ^{111}Ag , ^{127}Sb - $^{127(m)}\text{Te}$, ^{126}I , ^{131}I , ^{133}Xe , ^{136}Cs , ^{141}Ce , (^{143}Ce) - ^{143}Pr , ^{147}Nd - ^{147}Pm , ^{149}Pm , ^{153}Sm , ^{156}Eu , ^{159}Gd and ^{161}Tb could be used as γ tracer for the diagnostic of specific organs and/or as specific β source for radio-therapy of targeted organs. Among them lanthanide radioisotopes are of great interest because of their formation with bio-specific ligands of very stable complexes, e.g. terbium (^{149}Tb , ^{152}Tb , ^{155}Tb , and ^{161}Tb), see Naskar & Lahiri (2021) [5]. They are anticipated to be cheaper than those produced by irradiation using an accelerator or a research reactor because of their expensive irradiations for their production.

This paper explores the use of fission products isotopes selected for radio-diagnostics but also for β^- radiotherapy of bacterial or viral diseases.

2. Fission product radioisotope production from Molten Salt Reactors

The classical Molten Salt Reactors (MSRs) use liquid fuel, which in their classical MSR design, is also the coolant. They were intensively investigated at the Oak Ridge National Laboratory e.g. Weinberg (1979) [6] which initiated the scientific basis of the MSRs. Compared to the light water reactors (LWR), these reactors are safer as reported by reactor safety experts e.g. Elsheikh (2013) [7]. In addition, they run with larger EROEI factor (around 1000) than the commercial LWR (110-11) as evaluated by Huke, *et al.* (2015) [8]. Their implantation as Small Modular Reactors (SMRs) was suggested by Zou, *et al.* (2020) [9], and by Kang, *et al.* (2020) [10]. A specific nuclear fuel cycle was subsequently proposed by Degueldre, *et al.* (2019) [11] upgrading the system from sustainable to renewable. The SM-MS Reactor (see **Fig. 1**) targets optimisation for flexible reactor operation and energy production. With the actinide solubility increase in alkaline/earth alkaline chloride molten salt at high temperature, the build-up of neutron absorbers e.g. Xe, Nd, Pm, Sm, Eu and Gd isotopes generated as fission products degrade the neutron economy.

During MSR operation, the generated fission products flow from the reactor core along the primary loop. Radioisotopes of interest may be harvested. Their father nuclides e.g. ^{99}Mo with its half-life of 6.0 hours contributes to $^{99\text{m}}\text{Tc}$ concentration build-up. Similarly, the isotope ^{149}Pm generates ^{149}Sm , which has a neutron capture cross section of 40'100 barns and its elimination is also desirable. The behaviours and properties of Sr & Y, as well as Ln & Ln' in fluoride and chloride molten salts have been investigated by Smirnov, *et al.* (1988) [12]. Clearly, isotopes of Ln (Pm, Sm, Eu, Gd) as well as Xe are acting as neutron poisons and may require high fissile loading which may be costly. This affects reactor reactivity and reduce the energy production such as for ^{135}Xe as reported by Eades, *et al.* (2016) [13]. The case of ^{133}Xe has been treated recently, see Degueldre, *et al.* (2021) [18] revealing the flexibility of such an isotope for diagnostic and radiotherapy. In the case of Sr, ^{90}Sr decays in $^{90\text{m}}\text{Y}/^{90}\text{Y}$ and even if there are no such poisoning effect reported, these Y isotopes can also be used for diagnostic and radiotherapy e.g. Cheneler, *et al.* (2015) [14].

Several methodologies to eliminate strong Ln and Xe absorbers may be applied. Among them, decay process, degassing or ventilation treatment are suggested. The fraction of the absorbers which are entrained in the flowing molten salt mix, may be evaluated for given burn-up. A fast circulation of fuel salt decrease the fraction of ^{135}I and ^{135}Xe . Similarly ${}_z\text{Ln}$ decaying in ${}_{z-1}\text{Ln}$ which is of interest in this study can after collection of the absorber isotopes be separated from other isotopes by decay (see isotope half-life's in **Table 1**, Section 3). A high temperature may be needed. The second option is to ventilate the fluid with helium (less soluble) to remove the most volatile chlorides.

The release of fission products from MSR fuel under high temperature conditions has been studied by Kalilainen, *et al.* (2020) [15] coupled with computer simulations. The thermodynamic modelling of the fission product in the molten salt was achieved using GEMS (Gibbs Energy Minimization Software). The simulated fuel salt was LiF-ThF₄-UF₄ with Cs and I as fission products. Experimental results were compared to simulations considering pure compound vapour pressures. The salt mixing effects, when compared to the pure compound simulation affect evaporation conditions and therefore the kinetics of the release of compounds. The analysis was performed by mass spectroscopy; a more sensitive than that reported earlier

by Akerib, *et al.* (2018) [16]. Lanthanide extraction is consequently recommended in the primary loop. **Figure 1** presents a schematic picture of the SM-MSR including the module for the treatment of fission products (FP absorber) and from where the collection of Sr and Ln is carried out.

The potential for medical applications of produced MSR specific fission product isotopes, e.g. ^{90m}Y and ^{99m}Tc , must be re-explored such as bone and liver imaging or radiotherapy must be revisited.

The production of ^{99}Mo in a 2 MW molten salt reactor using low-enriched uranium has been proposed by Yu, *et al.* (2020) [17] as source of ^{99m}Tc for radio-diagnostic. More recently, the production of ^{133}Xe from a fast molten salt reactor has been suggested for its versatile use for diagnostic and radiotherapy by Degueldre (2021) [18].

With its energy production and its isotope production line for short life fission products an MSR such as the IMSR may be adapted with an isotope extraction line on the left and bottom, original plant cross section from Terrestrial Energy as reported by LeBlanc (2018) [19].

Fig. 1. Simplified molten salt reactor (MSR), including the reactor core, the primary heat transfer loop, the secondary, and ternary loop.

3. Nuclear properties of fission product radioisotopes

For practical reasons, interest is set on isotopes with half-life larger than one day and smaller than ten days (see **Table 1**). Decay's nuclides include only β^- emitters since isotopes produced as fission products are generally heavier than the natural isotopes. Daughter products are added as they are potentially also radionuclides. They must be considered since they may have a radiotoxic activity. The nuclear properties of fission product isotopes produced by MSR guide us for their selection as radio-diagnostic and radio-therapy isotopes.

^{82}Br , ^{86}Rb , (^{90}Sr) - ^{90m}Y , (^{99}Mo) - ^{99m}Tc , ^{103}Ru - ^{103m}Rh , ^{111}Ag , ^{127}Sb - $^{127(m)}\text{Te}$, ^{126}I , ^{131}I , ^{133}Xe , ^{136}Cs , ^{141}Ce , ^{144}Ce , ^{143}Pr , ^{147}Nd - ^{147}Pm , ^{149}Pm , ^{153}Sm , ^{156}Eu , ^{159}Gd and ^{161}Tb .

Decay reactions are relisted below. The relevant physical data of the emitted particles are given in Table1.

One Br radioisotope decaying by: $^{82}\text{Br} \rightarrow \beta^- + \gamma + ^{82}\text{Kr}$.

One Rb radioisotope decaying by: $^{86}\text{Rb} \rightarrow \beta^- + \gamma + ^{86}\text{Sr}$.

One Sr radioisotope decaying by: $^{90}\text{Sr} \rightarrow \beta^- + \gamma + ^{90m}\text{Y} \rightarrow \gamma + ^{90}\text{Y} \rightarrow \beta^- + \gamma + ^{90}\text{Zr}$.

One Mo radioisotope decaying by: $^{99}\text{Mo} \rightarrow \beta^- + \gamma + ^{99m}\text{Tc} \rightarrow \gamma + ^{99}\text{Tc} \rightarrow \beta^- + \gamma + ^{99}\text{Ru}$.

One Ru radioisotope decaying by: $^{103}\text{Ru} \rightarrow \beta^- + \gamma + ^{103m}\text{Rh} \rightarrow \gamma + ^{103}\text{Rh}$.

One Ag radioisotope decaying by: $^{111}\text{Ag} \rightarrow \beta^- + \gamma + ^{111\text{m}}\text{Cd} \rightarrow \gamma + ^{111}\text{Cd}$.

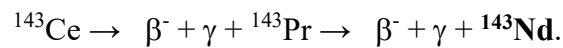
One Sb radioisotope decaying by: $^{127}\text{Sb} \rightarrow \beta^- + \gamma + ^{127\text{m}}\text{Te} \rightarrow \gamma + ^{127}\text{Te} \rightarrow \beta^- + \gamma + ^{127}\text{I}$.

One I radioisotope decaying by: $^{131}\text{I} \rightarrow \beta^- + \gamma + ^{131\text{m}}\text{Xe} \rightarrow \gamma + ^{131}\text{Xe}$. (^{126}I not considered).

One Xe radioisotope decaying by: $^{133}\text{Xe} \rightarrow \beta^- + \gamma + ^{133}\text{Cs}$.

One Cs radioisotope decaying by: $^{136}\text{Cs} \rightarrow \beta^- + \gamma + ^{133}\text{Ba}$.

Two Ce radioisotopes decaying by: $^{141}\text{Ce} \rightarrow \beta^- + \gamma + ^{141}\text{Pr}$, and



One Pr radioisotope decaying by: $^{143}\text{Pr} \rightarrow \beta^- + \gamma + ^{143}\text{Nd}$.

One Nd radioisotope decaying by: $^{147}\text{Nd} \rightarrow \beta^- + \gamma + ^{147}\text{Pm} \rightarrow \beta^- + \gamma + ^{147}\text{Sm}$.

One Pm radioisotope decaying by: $^{149}\text{Pm} \rightarrow \beta^- + \gamma + ^{149}\text{Sm}$.

One Sm radioisotope decaying by: $^{153}\text{Sm} \rightarrow \beta^- + \gamma + ^{153}\text{Eu}$.

One Eu radioisotope decaying by: $^{156}\text{Eu} \rightarrow \beta^- + \gamma + ^{153}\text{Gd}$.

One Gd radioisotope decaying by: $^{159}\text{Gd} \rightarrow \beta^- + \gamma + ^{159}\text{Tb}$.

One Tb radioisotope decaying by: $^{161}\text{Tb} \rightarrow \beta^- + \gamma + ^{161}\text{Dy}$

Among them, some e.g. ^{90}Y could be used as PET isotopes since their high γ energy allows formation of β^+ .

To complete the list of relevant physical properties, these short life fission product properties are also presented in **Table 1** for their fission production rate, half-life, specific activity, the energy of their gamma most intensive lines (for diagnostic), the maximum beta energy and average beta energy for radiotherapy.

Table 1: Nuclear properties of fission product radioisotopes released from MSR and of interest for nuclear medicine These isotopes are: ^{82}Br , ^{86}Rb , (^{90}Sr) - $^{90\text{m}}\text{Y}$, (^{99}Mo) - $^{99\text{m}}\text{Tc}$, ^{103}Ru - $^{103\text{m}}\text{Rh}$, ^{111}Ag , ^{127}Sb - $^{127\text{(m)}}\text{Te}$, ^{126}I , ^{131}I , ^{133}Xe , ^{136}Cs , ^{141}Ce , ^{143}Ce , ^{143}Pr , ^{147}Nd - ^{147}Pm , ^{149}Pm , ^{153}Sm , ^{156}Eu , ^{159}Gd and ^{161}Tb . Note $T_{1/2}$ 2 days = 1.728×10^5 sec. Φ number of atom for 100 fission (%), Ref NEA (2022) [20]; λN (TBq mg^{-1}) optimal around 10 physical properties as given by Pfenning, *et al.* (1998) [21] and Holden (2004) [22], re-actualised data: ICPR (2008) [23]. Fission rate: black large, grey lower, light grey very low.

Isotope	Φ (%)	$T_{1/2}$ (s)	λN (TBq mg^{-1})	E_γ (keV)	$E_{\beta\text{Max}}$ (MeV)	$E_{\beta\text{Av}}$ (MeV)
^{82}Br	0.00066	1.271×10^5	40.1	776	2.32 - 0.4	0.143
^{86}Rb	0.00011	1.611×10^6	3.02	1077	1.77	0.067
^{90}Sr	5.73	9.085×10^8	0.005	-	0.546	0.196
$^{90\text{m}}\text{Y}$	0.0006	1.148×10^4	404.3	2319	0.643	0.232
^{90}Y	5.73	2.308×10^5	20.1	2186	2.28	0.931
^{99}Mo	6.13	2.374×10^5	17.8	740	1.21	0.389
$^{99\text{m}}\text{Tc}$	5.40	2.165×10^4	195	89.6 322	0.436	0.114
^{99}Tc	6.13	6.662×10^{12}	6.34×10^{-7}	89.5	0.293	0.101
^{103}Ru	3.10	3.400×10^6	1.2	497, 610	0.2, 0.76	0.063
$^{103\text{m}}\text{Rh}$	3.07	3.366×10^3	1205.	40	-	-
^{103}Rh	3.10	stable	0	-	-	-
^{111}Ag	0.02	6.437×10^5	5.85	342, 245	1.04	0.353
^{127}Sb	0.12	3.326×10^5	9.89	686,473,784	0.9, 1.5	0.309
^{127}Te	0.12	3.366×10^4	97.73	418	0.698	0.244
^{126}I	3.8×10^{-8}	1.132×10^6	2.97	389, 666	1.26	0.318
^{131}I	2.88	6.929×10^5	4.60	364, 637	0.6, 0.807	0.182
^{133}Xe	6.60	4.536×10^5	6.93	81	0.346	0.1
^{136}Cs	0.0058	1.137×10^6	2.70	819, 1048	0.3, 0.682	0.118
^{141}Ce	5.86	2.808×10^6	1.06	145	0.4, 0.581	0.145
^{143}Ce	5.95	1.189×10^5	24.6	293, 57	1.1, 1.46	0.406
^{143}Pr	5.95	1.172×10^6	2.49	742	0.934	0.315
^{147}Nd	2.23	9.487×10^5	3.00	91, 531	0.895	0.233
^{147}Pm	2.23	8.279×10^7	0.034	121	0.225	0.062
^{153}Sm	0.15	1.674×10^5	16.31	103, 70	0.808	0.223
^{156}Eu	0.013	1.313×10^6	2.04	812,89,1231	2.45	0.431
^{159}Gd	0.0011	6.652×10^4	39.5	364, 58	0.971	0.304
^{161}Tb	8.1×10^{-5}	5.967×10^5	4.35	26, 49, 75	0.593	0.154

For light and heavy fission product the fission yield for their production is rather low, restricting their production. The plot $E_{\beta\text{Max}}$ as a function of specific activity of the radionuclides was tested but no correlation was found as described in Degueldre (2017) [24] for the caesium isotopes maybe because the range of nuclide is too large.

4. Physical-chemical properties of fission product radioisotopes in the molten salt

The physical-chemical properties are important and must be considered to perform an efficient separation of the fission products. The thermodynamic data of the liquid fuel components and fission product as elements and their chlorides needed for the separation processes are given in **Table 2**. This table reveals what are the volatiles elements and chlorides and what are their densities. The noble metals are refractory with T_B going from 4639 to 2963°C for Mo to Pd and around 2000°C (except Cd) up to Sb. The density of these elements is above 10 g cm⁻³ from Mo to Pd and above 6.66 from Ag to Sb.

Table2: Thermophysical properties of metallic fission products (Fp) and selected chloride salts. Data from Yaws (2015)[25].

Fp	T_M °C	T_B °C	T_C , °C	α °C ⁻¹	$\rho(25^\circ\text{C})$ g cm ⁻³	$\rho(500^\circ\text{C})$ g cm ⁻³
Se	220	685	1493	2.1×10^{-6}	10.18	4.80
Mo	2623	4639	9347	3.0×10^{-6}	10.96	-
Tc	2157	4265	17127	7.1×10^{-6}	11.00	
Ru	2334	4150	14974	5.1×10^{-6}	12.10	12.07
Rh	1964	3697	12633	4.4×10^{-6}	12.45	12.42
Pd	1555	2963	10396	6.6×10^{-6}	12.00	11.96
Ag	962	2212	6137	11.0×10^{-6}	10.50	10.44
Cd	321	767	2018	16.8×10^{-6}	8.69	8.62
In	157	2072	6457	18.3×10^{-6}	7.31	7.25
Sn	232	2602	7127	12.8×10^{-6}	7.27	7.22
Sb	631	1587	4797	5.0×10^{-6}	6.68	6.66
Te	449.5	988	4567	20.5×10^{-6}	6.24	6.18
SeCl ₄	191.6	305	471	8.64×10^{-4}	2.60	1.72
RbCl	718	1390	2421	36.0×10^{-6}	2.76	2.71
SrCl ₂	873	1249	3030	2.41×10^{-4}	3.05	2.91
YCl ₃	721	1507	2560	2.66×10^{-4}	2.61	2.62
ZrCl ₃	627	330				
ZrCl ₄	437	331	505	-1.2×10^{-6}	2.80	2.80
NdCl ₅	205	254	530	7.98×10^{-4}	2.78	2.02
MoCl ₂	530	1427			3.71	
MoCl ₃	410				3.74	
MoCl ₄	552	322				
MoCl ₅	194	268	577	7.54×10^{-4}	2.93	2.16
TcCl ₃						
TcCl ₄		300				
RuCl ₂	194					
RuCl ₃	500				3.10	
RhCl ₃	450	717			5.38	
PdCl ₂	679				4.00	
AgCl	455	1547	2719	31.0×10^{-6}	5.56	4.83
CdCl ₂	564	960	1747	3.64×10^{-4}	4.08	3.45
InCl ₃	497	586	688	1.5×10^{-3}	4.00	2.31

SnCl ₂	247	623	1186	4.68×10 ⁻⁴	3.90	3.04
SbCl ₃	73	220	521	8.07×10 ⁻⁴	3.14	1.34
TeCl ₄	224	387	729	6.45×10 ⁻⁴	3.00	2.17
ICl	27	98				
CsCl	645	1297	2289	2.84×10 ⁻⁴	3.99	2.78
BaCl ₂	962	1560	3284	2.29×10 ⁻⁴	3.90	3.47
LaCl ₃	858	1000	2987	2.69×10 ⁻⁴	3.84	3.49
CeCl ₃	817	1727	2866	2.76×10 ⁻⁴	3.97	3.54
PrCl ₃	786	1710			4.02	
NdCl ₂	841					
NdCl ₃	758	1600			4.13	
PmCl ₃	737	1670				
SmCl ₂	855	1950			3.69	
SmCl ₃	682				4.46	
EuCl ₂	731	2190			4.90	
EuCl ₃	623				4.89	
Salt comp.						
NaCl	801	1465	3600	44.0×10 ⁻⁶	2.17	2.12
RbCl	718	1390	2421	36.0×10 ⁻⁶	2.76	2.71
UCl ₃	837	1657		1.57×10 ⁻⁴	5.51	5.13
UCl ₄	590	791	1388	42.0×10 ⁻⁵	4.87	4.06
UCl ₅	287				3.81	
UCl ₆	177	527			3.60	
PuCl ₃	760	1793			5.71	
PuCl ₄					4.72	
Salt mix.	T _{Eu}					
NaCl-UCl ₄	371				4.18	3.62
RbCl-UCl ₄					4.11	3.63

McFarlane, *et al.* (2020), Molten salt reactor engineering study of off-line gas management
ORNL TM – 2020 /1602

4.1 Partial pressure of molten salt components and fission products

For the investigation of a separation strategy it is important to compare, for the pure chloride compounds (MCl_x), the trends of their vapour pressure as a function of temperature. **Figure 2** displays the plots P(MCl_x) vs T for the investigated chlorides in order to estimate in a pragmatic way the potential of distillation of chlorides above the molten salt. The thermodynamic law dictating the phase (l) => (g) reads:

$$\Delta G^\circ = RT \ln K_{eq} \quad \text{with } K_{eq} = p(\text{MCl}_x) \quad (1)$$

This could be applied for the molten salt components as well as for the melt containing chlorides of the fission products. In a simplified way one may argue with the pure components in a first approach. Calculations may be carried out using FactSage e.g. Bale, *et al.* (2016) [26].

Figure 2 reveals that MoCl₅ and ZrCl₄ are already volatile at 400°C while MoCl₄ and TeCl₄ become volatile at 400°C. PuCl₄ would rapidly be volatile around 500°C while UCl₄ would distillate around 700°C. InCl₃ is volatile around 600°C while the other trivalent chlorides (YCl₃, RuCl₃, RhCl₃, CeCl₃, SmCl₃, UCl₃) display insignificant volatility with P < 10⁻⁴ bar up to

900°C. The vapour pressure of carrier salt components NaCl and RbCl are found below 10^{-2} bar around 800°C and 900°C for NaCl. Finally the divalent chlorides SrCl₂, PdCl₂, BaCl₂ and SmCl₂ are found below 10^{-4} bar at 900°C.

NaCl, KCl and MgCl₂ vapour pressures investigated by Beckmann & Ncube (2007) [27] shows that P(NaCl) and P(KCl) equal 1 bar around 1400°C and 10^{-2} bar around 900°C and that P(KCl) > P(NaCl) and P(MgCl₂) > P(NaCl) for this later temperature.

Fig. 2. Vapour pressure variation with temperature: $P(MCl_x) = f(T)$ for **a.** mono- and di-chlorides, **b.** tri-chlorides, and **c.** tetra- and penta- chlorides. Conditions: Data from FactSage Bale, *et al.* (2016).

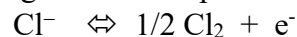
An equation for the vapour pressure of molten salts has been derived by Iida, *et al.* (1993) [28] combining the formula based on the harmonic oscillator model of a liquid with the modified Lindemann's equation. The values of the enthalpy of evaporation for various molten salts must be calculated from this equation using the experimental values of surface tension. The calculated values agreed well with the salt T_M and T_B : 1074 K and 1738 K for NaCl, 988 K and 1654 K for RbCl as pure compounds. This is also the case for CsCl. However it is difficult to validate it for ternary melts.

For UCl₃ one finds from Table 2 $T_M = 1,110$ K and $T_B = 1,930$ K, and for UCl₄ $T_M = 863$ K and $T_B = 1,064$ K. A pyrolytic separation of UCl₄ can be anticipated after oxidation of UCl₃. The evaporation of materials from the molten salt reactor fuel under elevated temperatures was recently reported by Kalilainen, *et al.* (2020) [29].

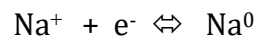
4.2 Redox properties of molten salt components and fission products

The redox potential domain available in the molten NaCl (LiCl or RbCl) salt is fixed between the most oxidizing half reaction couple and the most reducing one.

The half reactions ruling these redox potential writes:



For the most oxidizing couple in the molten salt and



for the most reducing one. The potential is reported vs the couple Cl⁻/Cl₂⁰ with acts as a reference.

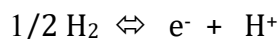
The reaction of the couple Cl⁻/Cl₂⁰ is used as a reference and per definition its redox potential E° equal 0 for $P = 1$ bar, see **Fig 3**. It is independent of the temperature and display the segment for $E^\circ = 0$ V. The apparent redox potential given by Nernst law writes:

$$E^{\circ'} = E^\circ + [RT/nF] \ln P(\text{Cl}_2) \quad (2)$$

And when the temperature and pressure of Cl₂ vary, it decreases consequently.

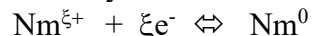
For the reducing domain and the most negative limit of potential the redox potential slightly increases with the temperature.

Another important redox reaction is that of the oxidation of H₂, a potential clean reagent. This reduction is guided by its half reaction redox potential couple based on the reactions:



Here again, when the temperature and pressure of H₂ vary, the redox potential change consequently. And the potential is reported vs the couple Cl⁻/Cl₂^o with act as a reference.

Now the metal ion Nm^{ξ+} may reduce according to the half reaction:



And its E^o between the potential of the couple Cl⁻/Cl₂^o and that of the couple Na^o/Na⁺ dictates its redox behaviour. A comparison of redox potentials for selected couples is given in **Fig. 3**.

The measurements of redox potential of uranium couples was performed in the 60ties by Caligara, *et al.* (1967) [30]. Data were revisited more recently in the temperature range 660–780 K. Two redox peaks were observed by Prabhakara, *et al.* (2004)[31] in the cyclic voltammograms corresponding to the two redox couples U(IV)/U(III) and U(III)/U which are found to be reversible and quasi-reversible. The reduction potentials of U(IV)/U(III) and U(III)/U are –0.325 and –1.490 V versus reference electrode (0.1 mol% AgCl in the LiCl–KCl) at 700 K.

The measurements of redox equilibrium of uranium ions were later performed for U⁴⁺ and U³⁺ in molten NaCl - 2CsCl at 923 K. A temperature dependence of the standard redox potential was found to be E^{o*}(U⁴⁺/U³⁺) (V) = –2.094 + 6.639×10⁻⁴ T (T = 823-923 K) as reported by Nagai, *et al.* (2005) [32]

Similarly, in the 400-550°C range, the electrochemical properties of uranium, dissolved in LiCl-KCl eutectic melt, were investigated by Masset, *et al.* (2005) [33] using transient electrochemical techniques. It was shown that U⁴⁺ is reduced to U⁰ by a two-step mechanism corresponding to U⁴⁺/U³⁺ and U³⁺/U⁰ couples. The apparent standard potentials of U⁴⁺/U³⁺ and U³⁺/U⁰ redox systems were E^{o*}(U⁴⁺/U³⁺) (V) = –1.902 + 0.0006104xT (K) vs. Cl₂/Cl⁻ and E^{o*}(U³⁺/U⁰)(V) = –3.099 + 0.0007689xT (K) vs. Cl₂/Cl⁻, or -2.543 V and -2.466 V vs Cl₂/Cl⁻ at 450°C and at 550°C respectively. YanHong *et al* (2017) [34] found similar reduction mechanism in NaCl–KCl.

This information shows that the production of U(IV) in the chloride salts is possible but that the electro-reduction of U³⁺ in U⁰ takes place slightly before Ln³⁺ in Ln⁰.

Similarly, in chloride salt molybdenum can be found on various valence states.

Molybdenum electrode and Mo(III)/(IV) redox potentials were measured in fused alkali chlorides by Volkovich, *et al.* (2017) [35]. Experiments were performed in individual salts (LiCl, NaCl, KCl, RbCl and CsCl) and in several binary and ternary eutectic or low-melting mixtures between 633 and 1173 K (depending on the melting point of the solvent salt). Formal standard electrode potentials E^{*}(Mo/Mo(III)) and redox potentials E^{*}(Mo(III)/Mo(IV)) in respect to Cl⁻/Cl₂ couple and Gibbs free energy change of formation of molybdenum(III) chloride in alkali chloride melts were calculated. Electronic absorption spectra of Mo(III) ions were recorded, and spectroscopic parameters of MoCl₆³⁻ complex ions determined.

Similarly, the redox potential of relevant metal couples in chloride salts was investigated as a function of temperature by Young & Sham (2018) [36]. The AgCl in molten LiCl-KCl redox potential correction (vs Cl₂/Cl⁻) was investigated by Zhang, *et al.* (2019) [37]. **Figure 3** gives

the trend for relevant couples including for H, Li, Na, Cl, Fe, Y, Zr, Mo, Ag, La, Nd and U using also data from Koyama, *et al.* (1997) [38].

In addition to these metals the noble metals (Tc, Ru, Rh, Pd, Ag, Sn/Sb) need to be considered. Nazanin, *et al.* (2019) [39] contributed to the speciation of Ru in molten chlorides. They found that negatively charged ruthenium clusters dispersed in molten NaCl are expected. The Ru clusters are charged by adding additional Na atoms to the molten salt. Usually, Ru clusters are not stable in the few atom limit compared to Ru atoms in bulk metallic Ru. Once reduced the noble metals precipitate because their densities, as element or intermetallic, are larger than the molten salt itself. Calculations carried at 500°C are given in Table 2. Data for the liquid fuel are provided by Deciatnik & Kamitchev (1979) [40]. Part of the noble metal may however be found as electroplated in the pipes of the primary loop.

Fig.3: Redox potential Vs temperature of relevant metal couples in chloride salts. Conditions Redox potentials (V) vs $E^0(\text{Cl}_2/\text{Cl}^-)$, adapted from Young & Sham (2018)[90] and Koyama, *et al.* (1997) [91].

5 Radioelement and radioisotope separation

Online reprocessing and refuelling are key processes for MSR as discussed by He *et al.* (2020)[41] for thorium – uranium breeding reactors. Similarly in the case of the uranium MCSFR, the fission products can be separated from the liquid fuel on the basis of their physical-chemical properties.

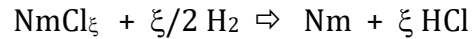
5.1 Separation of the fission gases

The separation of xenon and krypton gases from the molten salt fuel has been reported by Degueldre, *et al.* (2021)[18]. Their solubility in molten chloride decreases with temperature. This separation can consequently first be done after the reactor and can be completed at low temperatures after the heat exchanger reducing a second time the fraction of dissolved gases.

Separation of xenon and krypton carried out by distillation, e.g. Banerjee, *et al.* (2018) [42]. Adsorptions under pressure and temperature swings are efficient alternatives; in addition, membrane-based separations are physical sorption using specific porous adsorbents to preferentially adsorb xenon or krypton. The porous material has to be inert with the components of the molten salt.

5.2 Separation of metallic components from the molten salt fuel.

With burn up, the molten salt becomes $\text{NaCl} - \text{UCl}_3 - \text{UCl}_4 - \text{FpCl}_\xi$ with Fp stands for fission product from where noble metals (Nm: Tc, Ru, Rh, Pd and Ag, Cd, In, Sn, Sb) precipitate under reducing conditions such as 1% H_2 in Ar). The reaction ruling the reduction writes:

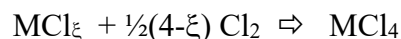


These reductions are driven by their E° values. Their comparison for the Nm series as a function of temperature is presented in Fig 3. At low temperature (e.g. 500°C) co-precipitations may take place with inter-metallic compounds such as NmU_3 .

The precipitation can be completed by adding H_2 excesses, producing elementary Mo, Ag, Cd, In and Sn. However, Sb, Te, I, Se and Br may form SbH_3 , TeH_2 , HI , SeH_2 and HBr respectively which can be collected sequentially.

5.3 Separation of the volatile chlorides

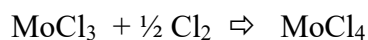
Penta- and tetra- valent fission products or actinides chlorides are rather volatile and can distillate or sublimate from the melt. Their oxidation reaction by chlorine writes:



More accurately, chlorides of elements with high valence states are usually more volatile than their low valence compounds. Table 2 shows that this is verified for MoCl_ξ and UCl_ξ . This is also true for SnCl_ξ (with $T_B \text{ SnCl}_4$: 114°C) and for chlorides from a same period: AgCl , CdCl_2 , InCl_3 and SnCl_4 .

ZrCl₃ which reacts with chlorine forming ZrCl₄ for which one finds (with T_M: 437°C and T_B: 331°C, see Table 2) undergoes evaporation from the molten chlorides.

Similarly, MoCl₃ formed in the molten salt can be oxidised according to:

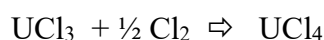


MoCl₄ with its T_M: 552°C and T_B: 322°C (see Table 2) can distillate from molten NaCl–KCl. Separation can consequently be performed according to the relative volatility of the tetrachlorides (see Fig. 2). Actually, molybdenum may react with chlorine in molten alkali metal chlorides between 400 and 700°C as investigated by Volkovicha, *et al.* (2003) [43] in the following melts: LiCl–KCl, NaCl–CsCl and NaCl–KCl. In these molten salts Mo reacts under 1% Cl₂ – Ar producing initially MoCl₆²⁻ and then a mixture of Mo(III) and Mo(V) chloride-complexes as described by Volkovicha, *et al.* (2003). With its low boiling point (T_B: 268°C, see Table 2) Mo(V) can be removed from the melt in the form of MoCl₅.

Technetium can also be oxidized as technetium tetra-chloride in the chloride melts and because of its low boiling point (T_B: 300°C, see Table 2) TcCl₄ can be extracted from the melt.

Similarly, tellurium tetrachloride with (T_B: 380°C, see Table 2) can be separated following an analogous protocol.

Finally, the uranium separation may be suggested by oxidising U(III) in U(IV) e.g. using Cl₂ diluted in Ar. Consequently the part of UCl₃ present in the molten salt may be oxidised according to



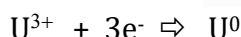
The Na(Rb)-UCl₄ binary mixture of the main components is easy to separate by distillation / vaporisation of UCl₄ that quit the molten salt and condensate in the form of UCl₄ crystals that can be recovered for reutilisation. It must be noted that the presence of ²³⁶UCl₄ and other tetravalent chlorides should degrade the uranium quality. And additional purification of UCl₄ is required prior recycling for use in MSR.

Separation includes first MoCl₄ followed by TcCl₄, ZrCl₄ and TeCl₄. Actinides tetrachlorides (UCl₄, NpCl₄, PuCl₄, and AmCl₄) follow. An additional purification can also be carried out during condensation.

5.4 Separation by electro-reduction

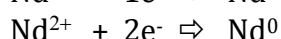
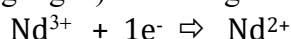
Specific voltammograms recorded for example for uranium in LiCl–KCl by Masset, *et al.* (2005) [88] and for neodymium in LiCl–KCl also by Kim & Lee (2020) [44] are shown in Fig 4. They show the waves generated by due to the electro-deposition of U⁰ and of Nd⁰.

As visible the electrodeposition of uranium is the first to take place on the voltammogram. The potential of electroreaction is –1.5 V (vs Ag/AgCl at 430°C) for:



Which is similar to the E° of the U^{3+/0} couple: 1.68 V vs Ag/AgCl (see data in Fig 6).

For Nd³⁺ the electroreductions in Nd²⁺ at -1.7 V is completed by the electrodeposition in Nd⁰ at -2.2 V vs Ag/AgCl) according to:



The electrodeposition of U can be discriminated from that of Nd.

Fig. 4

Comparison of cyclic voltammograms of NdCl_3 and of UCl_3 in LiCl-KCl eutectic molten salt Conditions:

for U^{3+}/U^0 redox system: on a tungsten electrode $S = 0.34 \text{ cm}^2$, at 430°C (703 K), counter electrode: Mo, reference electrode: Ag/AgCl 1 wt%, $\nu = 100 \text{ mV s}^{-1}$, $\text{U}^{3+} = 9.87 \times 10^{-5} \text{ mol cm}^{-3}$. Ref. Masset *et al* (2005).

for $\text{Nd}^{3+}/\text{Nd}^{2+}/\text{Nd}^0$ redox system of 4 wt% NdCl_3 in LiCl-KCl eutectic molten salt, $S = 0.21 \text{ cm}^2$, with scan rate $\nu = 100 \text{ mV s}^{-1}$ at 500°C (773 K). Ref. Kim & Lee (2020).

The electrochemical separation of actinides and lanthanides in molten chloride (LiCl–KCl) is possible as reported by Wang, *et al.* (2013) [45]. Based on the voltammogram of Ce^{3+} and the former result of U^{3+} the electrodeposition was determined to be -1.65 V (vs Ag/AgCl). Uranium metal was successfully deposited and separated from cerium. The separation factors of uranium/cerium on different recovery ratios were determined. Some co-electrodeposition on cerium in uranium was observed when increasing the initial concentration of U^{3+} in the melt.

Figure 5 shows the cell designed by Yan & Fray (2010) [46] that could be used for the separation. Separation could be performed in such a cell by selective electro-deposition at -1.5 V (for U) prior -2.3 V (for Nd) followed by electro-dissolution first at $-1,75 \text{ V}$ followed by the U electro-dissolution at -1.00 V vs Ag/AgCl reference at 500°C (773 K).

Fig. 5: Schematic diagram of combined molten salt electro-refining cell. Adapted from Yan & Fray (2010).

5.5 Separation of the other fission products

Separation of divalent elements such as Sr^{2+} and Ba^{2+} can be carried out together with trivalent elements such as La^{3+} , Ce^{3+} , Pr^{3+} , Nd^{3+} , Pm^{3+} , Sm^{3+} , Eu^{3+} , and Gd^{3+} . This separation can be done in aqueous solution (after dissolution of the salt in water) using ion chromatography as reviewed by Chen, *et al.* (2022) [47].

Presently, a variety of techniques have developed for the separation and recovery of rare earth elements, commonly used including chemical precipitation, ion exchange, solvent extraction, membrane separation, and adsorption, etc. At present, there are few reports on the comprehensive progress of all separation and purification technologies for a single rare earth element. Van de Voorde, *et al.* (2019) [48] summarized the latest developments in the separation of rare earth elements and evaluated the advantages and disadvantages of various process technologies, and prospects the development prospects of rare earth element separation technologies.

As reported by Van de Voorde, *et al.* (2019), ^{143}Pr , ^{149}Pm , ^{153}Sm , ^{165}Dy , ^{161}Tb , ^{166}Ho , ^{169}Er , ^{170}Tm and ^{177}Lu find application in radio-pharmacy and nuclear medicine because of their suitable decay properties. These radioisotopes are generally produced by neutron activation in research reactors. Radiochemical processing of the targets is required high purity sources. Target material can be recycled after processing of the radiopharmaceutical lanthanide isotopes.

5.6 Separation scheme fission products on the molten salt reactor

Small molten salt reactor (MSR) unit which includes the reactor core, the primary heat transfer loop and the molten salt drain tank, may be completed by the Xe, Kr, He degassing system, and further separation units as described in Section 5 These separation sections of the reactor consists of chemical (gaseous reagents) or electrochemical treatment sub-units as sketched Figure 6. These subunits should be used at line after replacement of spent fuel volume by fresh fuel. The fission products separated on site are subsequently purified prior production of the radiopharmaceutical product

Fig. 6. Simplified molten salt reactor (MSR), including the reactor core, the primary heat transfer loop, the molten salt drain tank, the Xe, Kr, He degassing system, followed by specific separations.

6. Discussion

6.1 Fission product utilisation

Utilisation of fission products is desirable in circular economy.

Today, about 10 thousand tons of spent fuels are discharged annually worldwide from nuclear power plants (mainly light water reactors). The potential offered by these used fuels to extract elements has been addressed by Bourg & Poinssot (2017) [49]. The only elements that could be of interest, would be some lanthanides and platinum group elements. However, the amount of lanthanide that could be recovered from used fuels would be less than 0.01% of the annual production from conventional mining. The drawback is that storages of say 50 years after separation would be necessary for some of them to get a radioactivity level lower than exemption limit.

The question discussed here is however: could molten salt nuclear fuel be considered as a source of nuclide for nuclear medicine and biology? The response is yes, but all the nuclides listed in the introduction **are not suitable....**

6.2 Fission product for medical application

Selected radionuclides from the fission product initial list:

^{82}Br , ^{86}Rb , (^{90}Sr) - $^{90\text{m}}\text{Y}$, (^{99}Mo) - $^{99\text{m}}\text{Tc}$, ^{103}Ru - $^{103\text{m}}\text{Rh}$, ^{111}Ag , ^{127}Sb - $^{127\text{m}}\text{Te}$, ^{126}I , ^{131}I , ^{133}Xe , ^{136}Cs , ^{141}Ce , ^{143}Ce , ^{143}Pr , ^{147}Nd - ^{147}Pm , ^{149}Pm , ^{153}Sm , ^{156}Eu , ^{159}Gd and ^{161}Tb , have to be reconsidered. For commercial reason some have to be rejected because their production yield

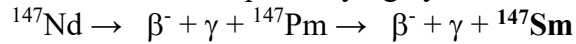
is below 0.02% (see Table 1), namely: ^{82}Br , ^{86}Rb , ^{111}Ag , ^{126}I , ^{136}Cs , ^{156}Eu , ^{159}Gd and ^{161}Tb ; some with specific activity below 2 TBq mg⁻¹ (see Table 1) are less attractive e.g. ^{90}Sr , ^{99}Tc , ^{103}Ru , ^{141}Ce , ^{147}Pm (and its father ^{147}Nd).

The remaining isotopes are then:

$^{90\text{m}}\text{Y}$, $^{99\text{m}}\text{Tc}$, $^{103\text{m}}\text{Rh}$, ^{127}Sb - $^{127\text{m}}\text{Te}$, ^{131}I , ^{133}Xe , ^{143}Ce , ^{143}Pr , ^{149}Pm and ^{153}Sm . Which is our basic list of fission product for medical application.

Their extraction from the spent fuel can be seen as a reprocessing which is beneficial when recycling the liquid fuel.

As an example, one of the Nd radioisotope decaying by:



produces during burn-up ^{147}Nd which acts as a poison according to:



Its cross section for neutron capture is 400 b which reduces its production. Several of these fission products behaves similarly and should be separated from the spent fuel for improving the neutron economy.

6.3 Application coupling radio-diagnostic and radiotherapy

In human body, **radio-diagnostic** is limited by the energy of the emitted gamma limiting their used in thick organ or broad body cross section. A precise assessment of the radioisotopes location and distribution in the treated organ is required prior full **radio-diagnostic** and coupled **radio-therapeutic** processes. Photon ($-X$ and γ spectra) are first recorded to quantify fractions (using gamma data) and for the estimation of in situ doses (using beta data) for example as reported by McIntyre, *et al.* (2016) [50] for radio-xenon. This combination allows full quantification of the doses of Ln radioisotope in-situ. The gamma spectra gained, as reported by McIntyre, *et al.* (2016), for large scintillation crystal, record the activity associated within the treated organ as estimated from the **gamma** peak. Once assessment of radio-lanthanide's is performed, radiography and tomography may be carried out to fully image the distribution.

For **radiotherapy**, the selection of the fission product radioisotope may be justified as follows. For nano- and micro- objects to treat (e.g. viruses, bacteria's, malign cell's), the object size must be larger than the free pathway of the **beta** when the emitter is sitting at the surface or inside the object. Recently Incerti, *et al.* (2018) [51] simulated β^- mean free pathways for their energy. Calculations were carried out using Geant4DNA applied for simulations in liquid water as a surrogate of biomaterial (viruses, bacteria's, malign cells). Actually, the mean β^- free pathway in water is a precious parameter to estimate the distance between successive interactions, it may be used to select the β emitter energy in radiotherapy.

To apply this concept for the selected radionuclide its $E_{\beta\text{mean}}$ should range from 0.10 to 0.40 MeV. The selected nuclides are then:

$^{90\text{m}}\text{Y}$ (0.23), $^{99\text{m}}\text{Tc}$ (0.11), $^{103\text{m}}\text{Rh}$ (γ only), ^{127}Sb (0.31) - $^{127\text{m}}\text{Te}$ (0.24), ^{131}I (0.18), ^{133}Xe (0.1), ^{143}Ce (0.41), ^{143}Pr (0.32), ^{149}Pm (1.1) and ^{153}Sm (0.22), with E_{β} (MeV).

6.4 Radiopharmaceutical reagent production

The reagents to prepare are ionic, complexes or nano-spheres.

The preparation of Y reagent e.g. Y_2O_3 **nanoparticles** is reported below. ^{90}Y as daughter product of ^{90}Sr must be intensively separated. A number of methods have been applied worldwide to separate carrier-free ^{90}Y from ^{90}Sr to clinical standards, including centrifugal extraction, see Srank, *et al.* (2010)[52], electrochemical separation, as reported by Chakravarty, *et al.* (2008)[53], supported liquid membrane (Kandwal, 2011)[54], precipitation (Chakravarty, *et al.* 2019)[55], and various forms of chromatography, see Hsieh, *et al.* (1993)[56] and Malja (2000)[57], amongst others.

^{90}Y is used in various forms in radiotherapy and imaging. For use in selective internal radiation therapy (SIRT - see section 2.4), ^{90}Y is often combined with resin (SIR-Spheres) or glass microspheres (TheraSphere), see Sundram, (2017)[58]. With the SIR-Spheres, a proprietary microsphere is coated with a partially cross-linked cation exchange polystyrene resin, into which ^{90}Y is attached through ion exchange of sodium for yttrium, followed by immobilisation via precipitation. For the TheraSphere, ^{89}Y is mixed with aluminium oxide and silicone dioxide and melted in a furnace. After cooling, the glass is crushed, spheridized through melting with a flame sprayer and sieved to size. Neutron bombardment of the spheres then converts the embedded ^{89}Y to ^{90}Y as reported by Westcott, (2016) [59].

Yttria is also a radiopharmaceutical precursor solution, i.e. an yttrium (^{90}Y) chloride solution, used for the in vitro radio-labelling of pharmaceutical substances or other chemical vectors for radio-immunotherapy, see Henke, *et al.* (2008)[60].

The preparation of lanthanide radiopharmaceutical reagents follows similar receipts e.g. Ln production in the form of Ln_2O_3 nanoparticles. Here the production follows a scheme as described for ^{90}Y e.g. glass particles as described by Cheneler & Ward (2015) [61]. This could be applied to ^{177}Lu or other radio-lanthanide as a source of gamma diagnostic.

Currently specific bioorganic complexes are used in radio-pharmacy.

Lanthanide (Ln) based complexes are appreciated in the medical field. Their applications have been reviewed by Chundawat *et al* (2021) [62] focusing on recent progress in developing lanthanide anticancer agents with an emphasis on lanthanide coordination complexes along these element series. Among them the Lu DOTA complex derivatives, e.g. Fig. 7, have received attention for their applications, e.g. see. Delbart *et al* (2021) [63]. The stability constants of complexes including ligands and lanthanides from La(III) to Lu(III) in water were studied by Bunzli & Pecharsky (2021)[64]. The lanthanide complexes with the (2.2.1) cryptand and the bibracchial lariat ethers (2.1)DA and (2.2)DA show little variation of their stability constant along the lanthanide series. A similar trend is expected for DOTA complexes with lanthanides, see **Fig 7**. Consequently, the Ce, Pr, Pm and Sm DOTA complexes could be more attractive than the ^{177}Lu DOTA complex for example. The best DOTA complex could be with ^{177}Lu however this radio-lutetium is not a fission product and its production is quite expensive.

Fig 7:

- a. Molecular structure of the **Lu DOTA** complex with its chelating ring. Adapted from Rinne et al (2019).

- b. The lanthanide (Ln) complexes with the (2.2.1) cryptand and the bibracchial **lariat ethers** (2.1)DA and (2.2)DA show little variation of their stability constants along the lanthanide series. Adapted from Bunzli & Pecharsky (2021) [116].

7. Conclusion

v. Single isotope production requires careful separation by evaporation/distillation, chemical reduction (using H₂ doped gas), electro-deposition and/or chemical oxidation (using Cl₂ doped gas). Refined isotope applications includes diagnostics using their emitted γ radiation or for specific cancers, bacterial or viral diseases radiotherapy using the emitted β^- particles. Among them ^{90m}Y, ^{99m}Tc, ^{103m}Rh, ¹²⁷Sb - ^{127m}Te, ¹³¹I, ¹³³Xe, ¹⁴³Ce, ¹⁴³Pr, ¹⁴⁹Pm and ¹⁵³Sm are selected for their use for radio-diagnostics thanks to their γ . Their use can also be extended to radiotherapy by utilising their 0.10 – 0.40 MeV β^- (E_{mean}). Now several fission product radioisotopes are produced together and since they have different nuclear properties, their separation is mandatory when one specific isotope has to be used. The present study promotes the use of the Molten Salt Reactor for the sustainable production of fission product radioisotopes for nuclear medicine coupling their use for radio-diagnostic and radiotherapy.

Acknowledgements

The present study was carried out in the frame of the MSR program which included the MS4MSR and the 0powerMSR chemistry (ZPR) projects at the Engineering Department of the Lancaster University. These projects are supported by Terrestrial Energy and Mitacs, Canada and by EPSRC, UK respectively. The authors acknowledge the discussion they had with Dr Chris Mayes, Head of the Nuclear Medicine Division of the University Hospital, University of Liverpool, UK.

References

- [1] Crestoni M. E.,
Radiopharmaceuticals for Diagnosis and Therapy
Reference Module in Chemistry, Molecular Sciences and Chemical Engineering. 2018,
M. E.
- [2] Baarsgaard Hansen S., Bender D.,
Advancement in production of radiotracers,
Seminars in Nuclear Medicine, 2021.
<https://doi.org/10.1053/j.semnuclmed.2021.10.003>
- [3] Bolus N., Glasgow K. W.,
Review of Nuclear Medicine Technology
5th edition, 2018, Society of Nuclear Medicine and Molecular Imaging.
ISBN: 978-0932004-95-6
- [4] Sun Z.,
Review: Production of nuclear medicine radioisotopes with ultra-intense lasers,
AIP Advances 11, 040701 (2021);
<https://doi.org/10.1063/5.0042796>
- [5] Naskar N., Lahiri S.,
Theranostic Terbium Radioisotopes: Challenges in Production for Clinical Application,
Front. Med., (2021).
<https://doi.org/10.3389/fmed.2021.675014>
- [6] Weinberg A. M.,
Can we fix nuclear energy?
Annals of Nuclear Energy. 6 (1979) 473-82.
[https://doi.org/10.1016/0306-4549\(79\)90019-7](https://doi.org/10.1016/0306-4549(79)90019-7)
- [7] Elsheikh B. M.,
Safety assessment of molten salt reactors in comparison with light water reactors,
Journal of Radiation Research and Applied Sciences, 6 (2013) 63-70.
<https://doi.org/10.1016/j.jrras.2013.10.008>
- [8] Huke A., Ruprecht G., Weißbach D., Gottlieb St., Hussein A., Czerski K.,
The Dual Fluid Reactor – A novel concept for a fast nuclear reactor of high efficiency,
Annals of Nuclear Energy, 80 (2015) 225-235.
<https://doi.org/10.1016/j.anucene.2015.02.016>
- [9] Zou Ch., Yu C., Wu J., Cai X., Chen J.,
Transition to thorium fuel cycle in a small modular molten salt reactor based on a batch reprocessing mode,
Annals of Nuclear Energy, 138 (2020) 107163,
<https://doi.org/10.1016/j.anucene.2019.107163>
- [10] Kang X., Zhu G., Yan R., Liu Y., Cai X.,
Evaluation of ⁹⁹Mo production in a small modular thorium based molten salt reactor,
Progress in Nuclear Energy, 124 (2020) 103337
<https://doi.org/10.1016/j.pnucene.2020.103337>
- [11] Degueldre C. A., Dawson R. J., Najdanovic-Visak V.,
Nuclear fuel cycle, with liquid ore and fuel: toward renewable.
Sustainable Energy & Fuels, 3 (2020) 1693-1700
<https://doi.org/10.1039/C8SE00610E>

-
- [12] Smirnov M. V., Korzun I. V., Oleynikova V. A.,
Hydrolysis of molten alkali chlorides, bromides and iodides,
Electrochim. Acta, 33 (1988) 781-788.
[https://doi.org/10.1016/S0013-4686\(98\)80007-8](https://doi.org/10.1016/S0013-4686(98)80007-8)
- [13] Eades M. J., Chaleff E. S., Venneri P. F., Blue Th.E.,
The influence of Xe-135m on steady-state xenon worth in thermal molten salt reactors,
Progress in Nuclear Energy, 93 (2016) 397-405.
<https://doi.org/10.1016/j.pnucene.2016.09.010>
- [14] Cheneler D., Ward M.,
Power output and efficiency of beta-emitting microspheres,
Radiation Physics and Chemistry, 106 (2015) 204-212,
<https://doi.org/10.1016/j.radphyschem.2014.07.019>
- [15] Kalilainen J., Nichenko S., Krepel J.,
Evaporation of materials from the molten salt reactor fuel under elevated temperatures,
Journal of Nuclear Materials 533 (2020) 152134.
<https://doi.org/10.1016/j.jnucmat.2020.152134>
- [16] Akerib D. S., Araújo H. M., Bai X., Bailey H. M., Zhang C.,
Chromatographic separation of radioactive noble gases from xenon,
Astroparticle Phys., 2018; 97 (2018) 80-87.
<https://doi.org/>
- [17] Yu Ch., Zou Ch., Wu Ch., Wu J., Cai X., Chen J.,
Sustainable supply of ⁹⁹Mo source in a 2 MW molten salt reactor using low-enriched uranium,
Applied Radiation and Isotopes, 160 (2020) 109134
<https://doi.org/10.1016/j.apradiso.2020.109134>
- [18] Degueldre C, Dawson R, Cooley I, Besley E . *Fission gas released from molten salt reactor fuel: the case of noble gas short life radioisotopes for radiopharmaceutical application*, Medicine in Novel Technology and Devices. Open access. . 10 (2021) 100057
<https://doi.org/10.1016/j.medntd.2021.100057>
- [19] LeBlanc D.,
Driving change with IMSR,
Nuclear Engineering International, 5 December 2018.
- 20 NEA JEFF-3.1.1 (2022)
- [21] Pfenning G., Klewe-Nebenius H., Seelmann-Eggebert W.,
Chart of the Nuclides,
Forschungszentrum Karlsruhe, (1998)
- [22] Holden N. E.,
*"11. Table of the Isotopes". In Lide, David R. (ed.).
CRC Handbook of Chemistry and Physics (85th ed.). Boca Raton, Florida: CRC Press. 2004. .*
- [23] ICPR (2008)
- [24] Degueldre C.,
The analysis of nuclear materials and their environments,
Springer, 2017.
- [25] Yaws C. L.,
The Yaws Handbook of Physical Properties for Hydrocarbons and Chemicals.

Gulf Professional Publishing 2015.

<http://dx.doi.org/10.1016/B978-0-12-800834-8.00002-5>

[26] Bale C. W., Bélisle E., Chartrand P., Deckerov S. A., Eriksson G., Gheribi A. E., Hack K., Jung I. H., Kang Y. B., Melançon J., Pelton A. D., Petersen S., Robelin C., Sangster J., Spencer P., Van Ende M.-A., *FactSage Thermochemical Software and Databases - 2010 - 2016*, Calphad, 54 (2016) 35-53
<https://doi.org/10.1016/j.calphad.2016.05.002>

[27] Beckmann M., Ncube S.,
Characterisation of Refuse Derived Fuels (RDF) in reference to the Fuel Technical Properties,
Proceedings of the International Conference on Incineration and Thermal Treatment Technologies - IT3, 14.05.-18.05.2007, Phoenix (USA).
ISBN 9780923204822

[28] Iida T., Kita Y., Morita Z.,
An Equation for Vapor Pressure and Its Application to Molten Salts,
ISIJ International, 33 (1993) 75-78.
<https://doi.org/10.2355/isijinternational.33.75>

[29] Kalilainen J., Nichenko S., Krepel J.,
Evaporation of materials from the molten salt reactor fuel under elevated temperatures,
Journal of Nuclear Materials; 533 (2020) 152134.
<https://doi.org/10.1016/j.jnucmat.2020.152134>

[30] Caligara F., Martinot L., Duyckaerts G.,
Contribution to the Knowledge of the Electrochemistry of Uranium in Molten LiCl-KCl Eutectic: I. The redox potential of the couple U(IV)/U(III),
Bulletin des Sociétés Chimiques Belges, 76 (1967) 5-14
<https://doi.org/10.1002/bscb.19670760102>

[31] Prabhakara B., Vandarkuzhali R. S., Subramanian T., Venkatesh P.,
Electrochemical studies on the redox mechanism of uranium chloride in molten LiCl-KCl eutectic,
Electrochimica Acta, 49 (2004) 2471-2478
<https://doi.org/10.1016/j.electacta.2004.02.002>

[32] Nagai T., Uehara A., Fujii T., Shirai O., Sato N., Yamana H.,
Redox Equilibrium of U⁴⁺/U³⁺ in Molten NaCl-2CsCl by UV-Vis Spectrophotometry and Cyclic Voltammetry.
Journal of Nuclear Science and Technology ; 42 (2005) 1025-1031
<https://doi.org/https://doi.org/10.1080/18811248.2005.9711055>

[33] Masset P., Bottomley D., Konings R., Malmbeck R., Rodrigues A., Serp J., Glatz J.-P.,
Electrochemistry of Uranium in Molten LiCl-KCl Eutectic,
Journal of The Electrochemical Society; 152 (2005) A1109-A1115.
<https://doi.org/10.1149/1.1901083>

[34] YanHong, J., Hui, H., Hui, Lin RuShan L., HongBin T.
Electrochemical behavior of uranium(III) in NaCl-KCl molten salt.
J Radioanal Nucl Chem, 311 (2017) 1763-1770.
<https://doi.org/10.1007/s10967-016-5131-8>

[35] Volkovich V. A., Ivanov A. B., Kamalov R. V., Maltsev D. S., Vasin B. D., Griffiths T. R.,
Electrode and Redox Potentials of Molybdenum and Stability of Molybdenum Chloro-Species in Alkali Chloride Melts.
Journal of The Electrochemical Society, 164 (2017) H5336 - H5344
<https://doi.org/10.1149/2.0511708jes>

[36] Young G. A., Sham S.,

Initial Assessment of Metallurgical Interaction of Clad/Base Metal Systems,
Sep 2018 ANL-ART-139 Argonne National Laboratory
<https://doi.org/10.2172/1506992>

[37] Zhang M., Ge J., Zhang J., Liu L. E.,
Redox potential measurement of AgCl in molten LiCl-KCl salt using chronopotentiometry and potentiodynamic scan techniques,
Electrochem., 105 (2019) 106498,
<https://doi.org/10.1016/j.elecom.2019.106498>

[38] T. Koyama, M. Iizuka, Y. Shoji, R. Fujita, H. Tanaka, T. Kobayashi, M. Tokiwai
An Experimental Study of Molten Salt Electrorefining of Uranium Using Solid Iron Cathode and Liquid Cadmium Cathode for Development of Pyrometallurgical Reprocessing,
Journal of Nuclear Science and Technology, 34 (1997) 384-393,
<https://doi.org/10.1080/18811248.1997.9733678>

[39] R. Nazanin, E. W. McFarland, H. Metiu, H. H. Kristoffersen.
Properties of Negatively Charged Ruthenium Clusters in Molten Sodium Chloride,
Journal of Physical Chemistry. C,; 123 (2019) .
<https://doi.org/10.1021/acs.jpcc.9b02616>

[40] Deciatnik V. N., Kamitchev C. F.,
Bulk and surface properties of NaCl – UCl₃ UCl₄ melts,
Ural Polytechnic Institute UDC 531.756 (1979) 1606-1610.

[41] He L.-Y., Li G.-Ch., Xia Sh.-P., Chen J.-G., Zou Y., Liu G.-M.,
Effect of ³⁷Cl enrichment on neutrons in molten chloride salt fast reactor.
Nucl. Sci. Tech. 31 (2020) 1-12.
<https://doi.org/10.1007/s41365-020-0740-x>

[42] Banerjee D., Simon C. M., Elsaidi S. K., Haranczyk M., Thallapally P. K.,
Xenon Gas Separation and Storage Using Metal-Organic Frameworks.
Chem., 4 (2018) 466–494.
<https://doi.org/10.1016/j.chempr.2017.12.025>.

[43] Volkovich V. A., Griffiths Tr. R., Thied R. C., Lewin B.,
Behavior of molybdenum in pyrochemical reprocessing: A spectroscopic study of the chlorination of molybdenum and its oxides in chloride melts,
Journal of Nuclear Materials, 323 (2003) 93-100.
<https://doi.org/10.1016/j.jnucmat.2003.08.039>.

[44] Kim S., Lee S.-H.,
Electrochemical Properties of NdCl₃ and CeCl₃ in Molten LiCl-KCl Eutectic Salt
Applied Sciences , 10 (2020) 7252;
<https://doi.org/10.3390/app10207252>

[45] Wang C. S., Liu Y., He H., Gao F. X., Liu L. S., Chang S. W., Guo J. H., Chang L., Li R. X., Ouyang Y. G.,
Electrochemical separation of uranium and cerium in molten LiCl-KCl,
Journal of Radioanalytical and Nuclear Chemistry, 298, (2013) 581–586.
<https://doi.org/10.1007/s10967-013-2506-y>

[46] Yan Y., Fray D.,
Molten salt electrolysis for sustainable metals extraction and materials processing a review,
Chap 5 in: Electrolysis: Theory, Types and Applications Editors: Shing Kuai and Ji Meng, pp, (2010) Nova Science Publishers, Inc.

- [47] Chen Z., Li Z., Chen J., Kallem P., Banat F., Qiu H.,
Recent advances in selective separation technologies of rare earth elements: a review,
Journal of Environmental Chemical Engineering, 10 (2022) 107104
<https://doi.org/10.1016/j.jece.2021.107104>
- [48] Van de Voorde M., Van Hecke K., Cardinaels Th., Binnemans K.,
Radiochemical processing of nuclear-reactor-produced radiolanthanides for medical applications,
Coordination Chemistry Reviews, 382, (2019) 103-125.
<https://doi.org/10.1016/j.ccr.2018.11.007>
- [49] Bourg S., Poinssot Ch.,
Could spent nuclear fuel be considered as a non-conventional mine of critical raw materials?
Progress in Nuclear Energy, 94 (2017) 222 - 228 .
<https://doi.org/10.1016/j.pnucene.2016.08.004>
- [50] McIntyre J. I., Schrom B. T., Cooper M. W., Prinke A. M., Suckow T. J., Ringbom A., Warren G. A.,
A program to generate simulated radioxenon beta-gamma data for concentration verification and validation and training exercises,
Journal of Radioanalytical and Nuclear Chemistry, 307 (2016) 2381-2387.
<https://doi.org/10.1007/>
- [51] Incerti S., Kyriakou I., Bernal M. A., Bordage M. C., Francis Z., Guatelli S., Ivanchenko V., Karamitros M., Lampe N., Lee S. B., Meylan S., Min C. H., Shin W. G., P. Nieminen P., D. Sakata D., Tang N., C. Villagrasa C., Tran H. N., Brown J. M. C.,
Geant4-DNA example applications for track structure simulations in liquid water: A report from the Geant4-DNA Project,
Medical Physics, 45 (2018).
<https://doi.org/10.1002/mp.13048>
- [52] J. Šrank, F. Melichar, A.T. Filyanin, M. Tomeš, M. Beran,
Preparation of $^{90}\text{YCl}_3$ radiopharmaceutical precursor for nuclear medicine using technology of centrifugal extractors.
Applied Radiation and Isotopes, 68 (2010) 2163-2168.
<https://doi.org/10.1016/j.apradiso.2010.07.012>
- [53] Chakravarty R., Pandey U., Manolkar, Dash A., Venkatesh M., Pillai M.A.,
Development of an electrochemical ^{90}Sr - ^{90}Y generator for separation of ^{90}Y suitable for targeted therapy.
Nuclear medicine and biology, 35 (2008) 245-253.
<https://doi.org/>
- [54] Kandwal P., Ansari S. A., Mohapatra P. K., Manchanda V. K.,
Separation of carrier free ^{90}Y from ^{90}Sr by hollow fiber supported liquid membrane containing bis (2-ethylhexyl) phosphonic acid.
Separation Science and Technology, 46 (2011) 904-911.
<https://doi.org/10.1080/01496395.2010.541402>
- [55] Chakravarty R., Chakraborty S., Jadhav S., Dash A.,
Facile radiochemical separation of clinical-grade ^{90}Y from ^{90}Sr by selective precipitation for targeted radionuclide therapy.
Nuclear medicine and biology, 68 (2019) 58-65.
<https://doi.org/10.1016/j.nucmedbio.2019.01.002>
- [56] Hsieh B. T., Ting G., Hsieh H. T., Shen L. H.,

Preparation of carrier-free yttrium-90 for medical applications by solvent extraction chromatography.
Applied radiation and isotopes, 44 (1993) 1473-1480.
[https://doi.org/10.1016/0969-8043\(93\)90101-F](https://doi.org/10.1016/0969-8043(93)90101-F)

[57] Malja S., Schomacker K., Malja E.,
Preparation of ^{90}Y by the ^{90}Sr - ^{90}Y generator for medical purpose.
Journal of Radioanalytical and Nuclear Chemistry, 245 (2000) 403-406.
<https://doi.org/10.1023/A:1006743428757>

[58] Sundram F. X., Buscombe J. R.,
Selective internal radiation therapy for liver tumours.
Clinical Medicine, 17 (2017) 449.
<https://doi.org/10.7861/clinmedicine.17-5-449>

[59] Westcott M. A., Coldwell D. M., Liu D. M., Zikria J. F.,
The development, commercialization, and clinical context of yttrium-90 radiolabeled resin and glass microspheres.
Advances in Radiation Oncology, 1 (2016) 351-364.
<https://doi.org/10.1016/j.adro.2016.08.003>

[60] Henke K. E., Beran M., Srank J., Melichar F.,
Quality control of no-carrier-added $^{90}\text{YCl}_3$ by estimating the labeling efficiency using its reaction with DOTATOC.
Journal of radioanalytical and nuclear chemistry, 278 (2008) 25-29.
<https://doi.org/10.1007/s10967-007-7186-z>

[61] D. Cheneler, M. Ward,
Power output and efficiency of beta-emitting microspheres,
Radiation Physics and Chemistry, 106 (2015) 204-212.
<https://doi.org/10.1016/j.radphyschem.2014.07.019>

[62] Chundawat N. S., Jadoun S., Zarrintaj P., Chauhan N. P. S.,
Lanthanide complexes as anticancer agents: A review
Polyhedron, 207 (2021) 115387
<https://doi.org/10.1016/j.poly.2021.115387>

[63] Delbart W., Ghanem G. E., Karfis I., Flamen P., Wimana Z.,
Investigating intrinsic radiosensitivity biomarkers to peptide receptor radionuclide therapy with [^{177}Lu]Lu-DOTATATE in a panel of cancer cell lines
Nuclear Medicine and Biology, 96–97 (2021) 68-79
<https://doi.org/10.1016/j.nucmedbio.2021.03.006>

[64] Bunzli J.-C. G., Pecharsky V. K.,
Handbook on the Physics and Chemistry of Rare Earths, 42 (2021): 9780444543165: Books
ISBN-10: 0444543163 Elsevier